

212316: sillimanite–cordierite–K-feldspar pelitic migmatite, Mount Joseph

(*Mount Joseph Migmatite, Marboo Formation, Western Zone, Lamboo Province*)

Korhonen, FJ, Romano, SS, Fielding, IOH, Kelsey, DE and Hollis, JA

Location and sampling

LENNARD RIVER (SE 51-8), RICHENDA (3963)

MGA Zone 51, 722726E 8078272N

WAROX site JBHLEN000225

Sampled on 21 July 2013

This sample was collected from low, bouldery outcrop to the west of a creek on Napier Downs Station, about 12.5 km north of Mount Behm, 2.4 km northeast of Mount Joseph Yard and 0.8 km southwest of Mount Joseph.

Geological context

The unit sampled is the Mount Joseph Migmatite, a component of the Marboo Formation in the Western Zone of the Lamboo Province (Tyler et al., 1999; Phillips et al., 2015). The Mount Joseph Migmatite consists of psammitic and pelitic migmatite, and anatectic granite formed by in situ melting of the Marboo Formation at high temperature and low pressure, probably driven by heat advected during regional-scale plutonic magmatism (Tyler et al., 1999; Phillips et al., 2015). A sample of Mount Joseph Migmatite, collected from the same locality as the sample reported here, yielded a conservative maximum depositional age of 1872 ± 8 Ma from zircon cores, and an age of 1865 ± 4 Ma for high-grade metamorphism from zircon rims (GSWA 212317, Fielding et al., 2020). A minimum age for deposition is provided by a crystallization age of 1864 ± 4 Ma for the Lennard Granite, which intrudes the Marboo Formation and Mount Joseph Migmatite (GA 8759.8011, Griffin et al., 2000). Monazite from the sample reported here yielded a date of 1827 ± 9 Ma (GSWA 212316, Fielding et al., 2019b), significantly younger than the zircon date of 1865 ± 4 Ma for metamorphic rims from the same locality. Monazite from a sample of Mount Joseph Migmatite about 1.7 km to the east yielded dates at 1854 ± 4 Ma and 1823 ± 6 Ma (GSWA 212305, Fielding et al., 2019a). The c. 1854 Ma age is interpreted as the timing of peak metamorphism (675–750 °C, 2.9 – 7.2 kbar; Korhonen et al., 2022), and the c. 1823 Ma age is attributed to an influx of fluids during deformation within the andalusite stability field (Korhonen et al., 2022).

Petrographic description

The sample is a sillimanite–cordierite–K-feldspar pelitic migmatite (Fig. 1), consisting of about 45% quartz, 19% K-feldspar, 11% biotite, 10% plagioclase, 8% cordierite, 7% sillimanite, trace ilmenite and muscovite, and accessory monazite and zircon (Fig. 2; Table 1). The sample is strongly layered and heterogeneous in grain size and mineral distribution, containing crudely aligned lenses of more coarsely grained quartz, plagioclase and K-feldspar separated by much finer grained aggregates of disseminated quartz, K-feldspar, cordierite, biotite, and sillimanite (Fig. 2). Elongate lenses of intergrown cordierite, biotite and sillimanite also occur (Fig. 3). Quartz is recrystallized, and up to 0.8 mm in diameter in the more coarsely crystalline leucocratic pods and lenses. K-feldspar is characterized by microperthite lamellae and scattered inclusions of round quartz. Cordierite occurs as large xenoblastic crystals up to 1.5 mm in diameter within the biotite–sillimanite-rich lenses (Fig. 3a), and contains numerous tiny round quartz and platy biotite inclusions. Disseminated cordierite within the finer grained matrix is commonly aligned. Reddish brown biotite forms small xenoblastic laths up to 0.8 mm long (Fig. 3b–d), although grains associated with the biotite–sillimanite-rich lenses can be up to 2 mm long (Fig. 3a). Sillimanite occurs as aligned, matted fibrolite

intergrown with biotite throughout the sample (Fig. 3), and is much coarser grained within the biotite–sillimanite aggregates. More rarely it also occurs as bladed grains up to 1 mm long or as square grains less than 0.1 mm across (Fig. 3a).



Figure 1. Outcrop image for sample 212316: sillimanite–cordierite–K-feldspar pelitic migmatite, Mount Joseph

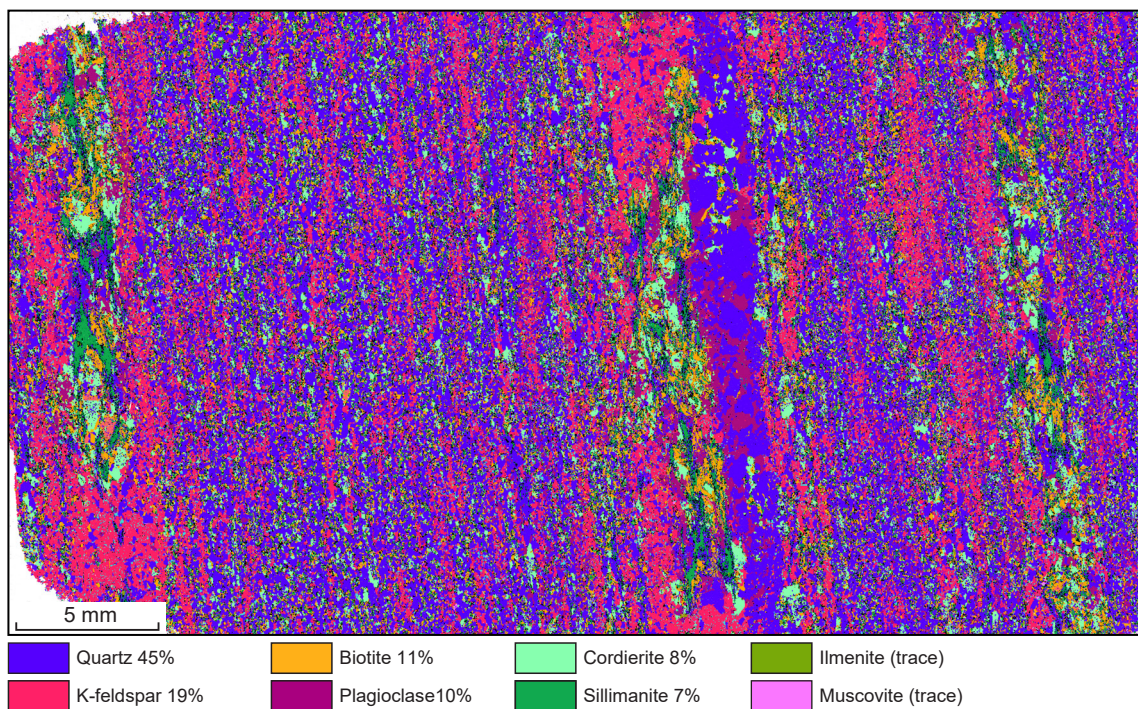


Figure 2. TESCAN Integrated Mineral Analyser (TIMA) image of an entire thin section from sample 212316: sillimanite–cordierite–K-feldspar pelitic migmatite, Mount Joseph. Volume percent proportions of major rock-forming minerals are calculated by the TIMA software

Table 1. Mineral modes for sample 212316: sillimanite–cordierite–K-feldspar pelitic migmatite, Mount Joseph

Mineral modes	Crd	Bt	Sil	Kfs	Pl	Ilm	Qz	Liq
Observed (vol%)	8	11	7	19	10	trace	45	–
Predicted (mol%)								
@ 3.5 kbar, 700 °C	trace	19	14	17	2	trace	44	4
@ 3.5 kbar, 730 °C	26	3	2	26	1	1	34	8
@ 2.9 kbar, 700 °C	26	3	2	26	1	1	34	7
@ 3.3 kbar, 700 °C	8	14	10	20	2	trace	41	5

NOTES: – not present

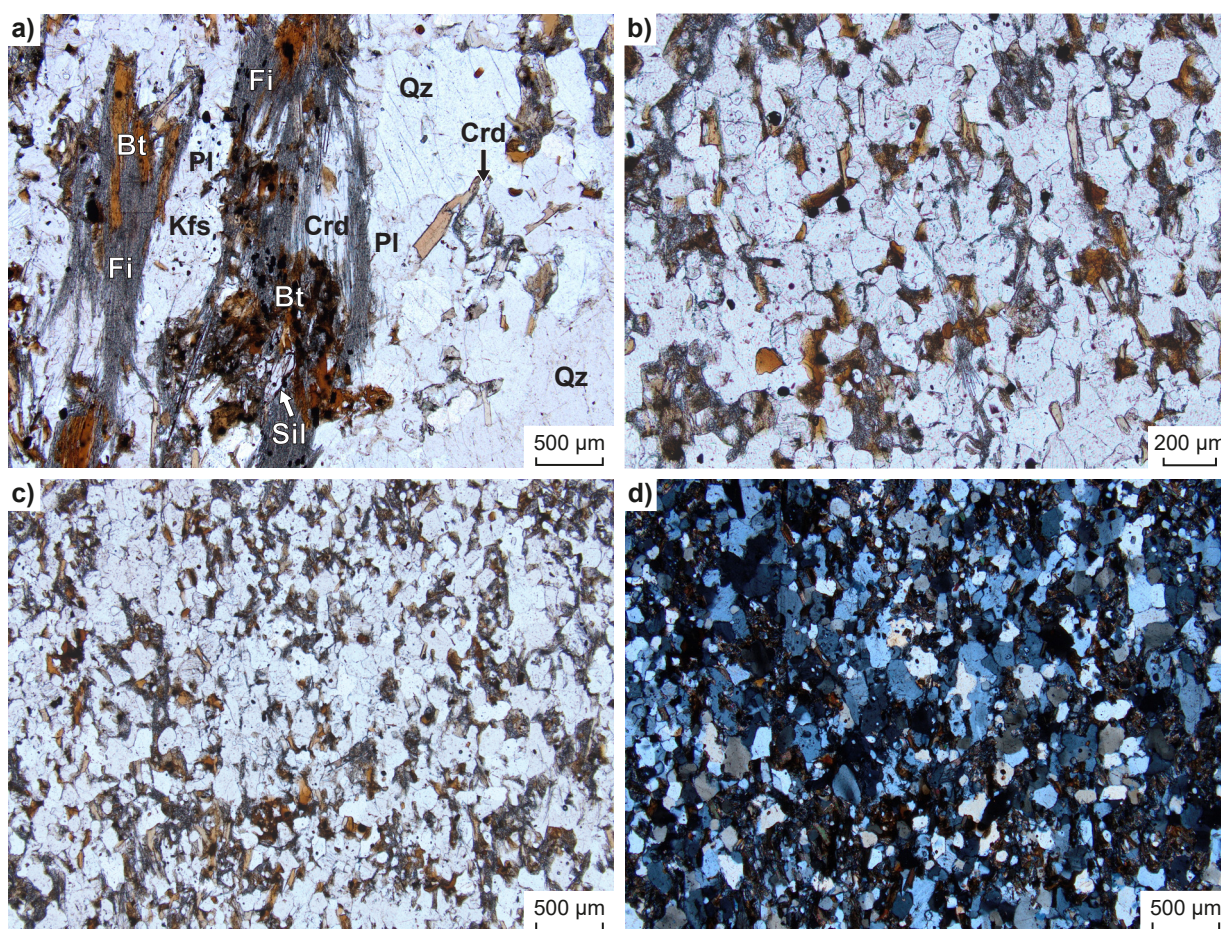


Figure 3. Photomicrographs, in plane-polarized light (a–c) and cross-polarized light (d), of sample 212316: sillimanite–cordierite–K-feldspar pelitic migmatite, Mount Joseph. Figures b–d show fine-grained matrix of disseminated quartz, K-feldspar, cordierite, biotite, and fibrolite. Abbreviations: Bt, biotite; Crd, cordierite; Fi, fibrolite; Kfs, K-feldspar; Pl, plagioclase; Qz, quartz; Sil, sillimanite

Table 2. Measured whole-rock and modelled compositions for sample 212316: sillimanite–cordierite–K-feldspar pelitic migmatite, Mount Joseph

<i>XRF whole-rock composition (wt%)(^a)</i>												
SiO ₂	TiO ₂	Al ₂ O ₃	Fe ₂ O ₃ ^(b)	FeO ^(b)	MnO	MgO	CaO	Na ₂ O	K ₂ O	P ₂ O ₅	LOI	Total
69.75	0.58	16.45	0.49	4.44	0.02	1.71	0.25	0.96	4.21	0.09	0.42	99.37
<i>Normalized composition used for phase equilibria modelling (mol%)</i>												
SiO ₂	TiO ₂	Al ₂ O ₃	O ^(c)	FeO ^{T(d)}	MnO	MgO	CaO ^(e)	Na ₂ O	K ₂ O	–	H ₂ O ^(f)	Total
74.59	0.47	10.37	0.20	4.37	0.02	2.73	0.15	1.00	2.87	–	3.25	100

NOTES:

- (a) Data and analytical details are available from the WACHEM database <<http://geochem.dmp.wa.gov.au/geochem/>>
(b) FeO analysed by Fe²⁺ titration; Fe₂O₃ content calculated by difference
(c) O content (for Fe³⁺) based on titration value
(d) FeO^T = moles FeO + 2 * moles O
(e) CaO modified to remove apatite: CaO(Mod) = CaO(Total) - (moles CaO(in Ap) = 3.33 * moles P₂O₅)
(f) H₂O content is LOI adjusted for oxidation state

Analytical details

The metamorphic evolution of this sample was investigated using phase equilibria, based on the bulk-rock composition (Table 2). The composition was determined by X-ray fluorescence spectroscopy, together with loss on ignition (LOI). FeO content was analysed by Fe²⁺ titration (as 91% of total Fe), and Fe₂O₃ calculated by difference. The modelled O content (for Fe³⁺) was derived from the titration value. The H₂O content was based on the measured amount of LOI, corrected for oxidation state. The bulk composition was corrected for the presence of apatite by applying a correction to calcium (Table 2). Thermodynamic calculations were performed in the MnNCKFMASHTO (MnO–Na₂O–CaO–K₂O–FeO–MgO–Al₂O₃–SiO₂–H₂O–TiO₂–O) system using THERMOCALC version tc340 (updated October 2013; Powell and Holland, 1988) and the internally consistent thermodynamic dataset of Holland and Powell (2011; dataset tc-ds62, created in February 2012). The activity–composition relations used in the modelling are detailed in White et al. (2014a,b). Additional information on the workflow with relevant background and methodology are provided in Korhonen et al. (2020).

Results

Metamorphic *P–T* estimates have been derived based on detailed examination of the thin section and the bulk-rock composition. The *P–T* pseudosection for this sample was calculated over a *P–T* range of 2–7 kbar and 600–800 °C (Fig. 4). The solidus is located between 665 and 710 °C across the range of modelled pressures, and is H₂O-saturated below 4.2 kbar. Garnet is stable at high temperatures (>740 °C) above 3.7 kbar. Cordierite is stable at lower pressure, with a maximum pressure stability of 5.1 kbar at 785 °C. Biotite is not stable in the low pressure–high temperature part of the diagram. K-feldspar is stable across the range of modelled conditions, and plagioclase is absent at high temperature. Muscovite is stable below the solidus above 4.1 kbar and at lower temperatures at lower pressure. Aluminosilicate-absent assemblages are predicted in the high temperature–low pressure part of the diagram above 730 °C, with a maximum pressure stability of 3.1 kbar at 800 °C.

Interpretation

The inferred peak assemblage of cordierite–biotite–sillimanite–K-feldspar–plagioclase–ilmenite–quartz–melt has a narrow stability field between 675 and 750 °C at 2.7 – 4.4 kbar (Fig. 4). The peak field is delimited by the presence of garnet at higher temperatures, the solidus at lower temperature, and the absence of cordierite at higher pressure. To lower pressures, magnetite is stabilized, followed by the loss of biotite.

Within the peak field, mineral modes change significantly over small changes in pressure and temperature. The predicted modes (molar proportions approximately equivalent to vol%) for cordierite, biotite, sillimanite and ilmenite are similar to the modes observed in the thin section (Table 1). Up to 8 mol% melt is predicted in the peak field, and the crystallization of melt during cooling could account for the higher modes of plagioclase and quartz preserved in the sample. There is no geochemical evidence for significant melt loss in the sample, suggesting that peak metamorphism may not have reached temperatures much higher than the solidus.

The fibrolite is interpreted to be post-peak, and must record a subsequent perturbation. However, it is difficult to determine if this growth occurred in the sillimanite or andalusite stability field, as the growth of metastable fibrolite in the andalusite stability field is well recognized (e.g. Kerrick, 1987), forming through the breakdown of biotite in the presence of fluids. The preferred interpretation is that the date of 1865 ± 8 Ma from zircon rims records melt crystallization following peak metamorphism, and the monazite date of 1827 ± 9 Ma corresponds to an influx of fluids and the growth of fibrolite.

Peak metamorphic conditions are estimated at 675–750 °C and 2.7 – 4.4 kbar, with an apparent thermal gradient between 170 and 250 °C/kbar. The absence of significant melt loss may suggest that peak metamorphic conditions were close to the solidus at pressures less than 3 kbar, corresponding to the higher apparent thermal gradients. These estimates are consistent with ultrahigh *T/P* conditions (see Korhonen et al., 2020), likely related to the heat advected during regional magmatism. There is no information on the prograde segment of the *P–T* path. An influx of fluids following peak metamorphism accounts for the growth of fibrolite, but the *P–T* conditions of this event are unconstrained.

References

- Fielding, IOH, Wingate, MTD, Lu, Y, and Hollis, JA 2020, 212317: pelitic migmatite, Mount Joseph; Geochronology Record 1624: Geological Survey of Western Australia, 8p.
- Fielding, IOH, Wingate, MTD, Lu, Y, Korhonen, FJ and Hollis, JA 2019a, 212305: pelitic migmatite, Mount Joseph; Geochronology Record 1620: Geological Survey of Western Australia, 5p.
- Fielding, IOH, Wingate, MTD, Lu, Y, Korhonen, FJ and Hollis, JA 2019b, 212316: pelitic migmatite, Mount Joseph; Geochronology Record 1623: Geological Survey of Western Australia, 5p.
- Griffin, TJ, Page, RW, Sheppard, S and Tyler, IM 2000, Tectonic implications of Palaeoproterozoic post-collisional, high-K felsic igneous rocks from the Kimberley region of northwestern Australia: Precambrian Research, v. 101, p. 1–23.
- Holland, TJB and Powell, R 2011, An improved and extended internally consistent thermodynamic dataset for phases of petrological interest, involving a new equation of state for solids: Journal of Metamorphic Geology, v. 29, no. 3, p. 333–383.
- Kerrick, DM 1987, Fibrolite in contact aureoles of Donegal, Ireland: American Mineralogist, v. 72, p. 240–254.
- Korhonen, FJ, Kelsey, DE, Fielding IOH and Romano, SS 2020, The utility of the metamorphic rock record: constraining the pressure–temperature–time conditions of metamorphism: Geological Survey of Western Australia, Record 2020/14, 24p.
- Korhonen, FJ, Romano, SS, Fielding, IOH, Kelsey, DE and Hollis, JA 2022, 212305: andalusite–sillimanite pelitic migmatite, Mount Joseph; Metamorphic History Record 13: Geological Survey of Western Australia, 9p.
- Phillips, C, de Souza Kovacs, N and Hollis, JA 2015, Richenda, WA Sheet 3963: Geological Survey of Western Australia: 1:100 000 Geological Series.
- Powell, R and Holland, TJB 1988, An internally consistent dataset with uncertainties and correlations: 3. Applications to geobarometry, worked examples and a computer program: Journal of Metamorphic Geology, v. 6, no. 2, p. 173–204.
- Tyler, IM, Page, RW and Griffin, TJ 1999, Depositional age and provenance of the Marboo Formation from SHRIMP U–Pb zircon geochronology: implications for the early Palaeoproterozoic tectonic evolution of the Kimberley region, Western Australia: Precambrian Research, v. 95, p. 225–243.
- White, RW, Powell, R, Holland, TJB, Johnson, TE and Green, ECR 2014a, New mineral activity–composition relations for thermodynamic calculations in metapelitic systems: Journal of Metamorphic Geology, v. 32, no. 3, p. 261–286.
- White, RW, Powell, R and Johnson, TE 2014b, The effect of Mn on mineral stability in metapelites revisited: New *a–x* relations for manganese-bearing minerals: Journal of Metamorphic Geology, v. 32, no. 8, p. 809–828.

Links

[Record 2020/14 The utility of the metamorphic rock record: constraining the pressure–temperature–time conditions of metamorphism](#)

Recommended reference for this publication

Korhonen, FJ, Romano, SS, Fielding, IOH, Kelsey, DE and Hollis, JA 2022, 212316: sillimanite–cordierite–K-feldspar pelitic migmatite, Mount Joseph; Metamorphic History Record 22: Geological Survey of Western Australia, 6p.

Data obtained: 6 November 2018

Date released: 7 October 2022

This Metamorphic History Record was last modified on 5 October 2022

Grid references in this publication refer to the Geocentric Datum of Australia 1994 (GDA94). All locations are quoted to at least the nearest 100 m.

WAROX is GSWA's field observation and sample database. WAROX site IDs have the format 'ABCXXXnnnnnnSS', where ABC = geologist username, XXX = project or map code, nnnnnn = 6 digit site number, and SS = optional alphabetic suffix (maximum 2 characters).

Isotope and element analyses are routinely conducted using the GeoHistory laser ablation ICP-MS and Sensitive High-Resolution Ion Microprobe (SHRIMP) ion microprobe facilities at the John de Laeter Centre (JdLC), Curtin University, with the financial support of the Australian Research Council and AuScope National Collaborative Research Infrastructure Strategy (NCRIS). The TESCAN Integrated Mineral Analyser (TIMA) instrument was funded by a grant from the Australian Research Council (LE140100150) and is operated by the JdLC with the support of the Geological Survey of Western Australia, The University of Western Australia (UWA) and Murdoch University. Mineral analyses are routinely obtained using the electron probe microanalyser (EPMA) facilities at the Centre for Microscopy, Characterisation and Analysis, UWA, at Adelaide Microscopy, University of Adelaide, and at the Electron Microscopy and X-ray Microanalysis Facility, University of Tasmania.

Digital data related to WA Geology Online, including geochronology and digital geology, are available online at the Department's [Data and Software Centre](#) and may be viewed in map context at [GeoVIEW.WA](#).

Disclaimer

This product uses information from various sources. The Department of Mines, Industry Regulation and Safety (DMIRS) and the State cannot guarantee the accuracy, currency or completeness of the information. Neither the department nor the State of Western Australia nor any employee or agent of the department shall be responsible or liable for any loss, damage or injury arising from the use of or reliance on any information, data or advice (including incomplete, out of date, incorrect, inaccurate or misleading information, data or advice) expressed or implied in, or coming from, this publication or incorporated into it by reference, by any person whosoever.



© State of Western Australia (Department of Mines, Industry Regulation and Safety) 2022

With the exception of the Western Australian Coat of Arms and other logos, and where otherwise noted, these data are provided under a Creative Commons Attribution 4.0 International Licence. (<http://creativecommons.org/licenses/by/4.0/legalcode>)

Further details of geoscience products are available from:

Information Centre
Department of Mines, Industry Regulation and Safety
100 Plain Street
EAST PERTH WA 6004
Telephone: +61 8 9222 3459 | Email: publications@dmirs.wa.gov.au
www.dmirs.wa.gov.au/GSWApublications